THE JOURNAL OF PHYSICAL CHEMISTRY C

Article

pubs.acs.org/JPCC

Electronic Polarization Effects upon Charge Injection in Oligoacene Molecular Crystals: Description via a Polarizable Force Field

Sean M. Ryno,[†] Stephen R. Lee,[†] John S. Sears,[†] Chad Risko,*[,†] and Jean-Luc Brédas*[,†,‡]

[†]School of Chemistry and Biochemistry and Center for Organic Photonics and Electronics, Georgia Institute of Technology, Atlanta, Georgia 30332-0400, United States

Supporting Information

ABSTRACT: Understanding the nature and magnitude of the electronic polarization due to the presence of a charge carrier in organic molecular solids is of fundamental importance in the description of charge-carrier transport. We present an approach to study these effects based on a polarizable force field that accounts for charge, dipole, quadrupole, and induced-dipole interactions. To demonstrate its general applicability, the method is applied to the oligoacene crystal series (naphthalene through pentacene) and perfluorinated derivatives of naphthalene and pentacene. Very good qualitative agreement with experimental results is achieved in terms of both the magnitude and asymmetry of the polarization as a function of the sign of the injected charge, with improved quantitative agreement versus previous theoretical assessments.

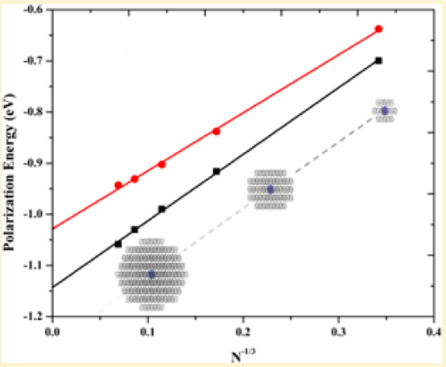

1. INTRODUCTION

Organic materials based on π-conjugated molecules and polymers have garnered considerable interest as the active layers in crystalline and thin-film electronic and electro-optic applications.[1−6] Regardless of the device architecture and function, the rates of charge-carrier transport generally constitute a determining factor in device efficiency and are intimately dependent on (i) the strength of electronic couplings between adjacent molecules, (ii) the extent of geometric and lattice relaxation upon ionization (for both oxidation and reduction), and (iii) differences in the site energies (i.e., the variations in the molecular ionization potentials and electron affinities). Importantly, these parameters, and in particular the latter, are influenced by polarization effects in the solid-state environment.[7−12]

The energetics of the polarization process, described here for the sake of example for a positive charge (cation or positive polaron), P_+, in a bulk material are generally defined by the Lyons relation:[7,8]

$$P_+ = \mathrm{IP}_{\mathrm{solid\ state}} - \mathrm{IP}_{\mathrm{gas\ phase}} \quad (1)$$

which simply represents the difference in the ionization potential of a molecule measured independently in the solid state ($\mathrm{IP}_{\mathrm{solid\ state}}$) and the gas phase ($\mathrm{IP}_{\mathrm{gas\ phase}}$). Gas-phase and solid-state ultraviolet photoelectron spectroscopies (UPS) are generally used in combination to obtain a measure for P_+, which for a large number of π-conjugated organic molecules is on the order of 1.5−2.0 eV.[9−11] A similar relation holds for the polarization energy (P_-) induced by a negative charge (anion or negative polaron), typically around 1.1 eV for organic semiconductor materials,[10] and is a function of the electron affinity differences in the solid state vs the gas phase.

The polarization energy, P, can be understood at an even more fundamental level by considering the underlying physical mechanisms of the phenomenon through the relation:[12,13]

$$P = E_{\mathrm{nuc}} + E_{\mathrm{dip}} + E_{\mathrm{qQ}} + E_{\mathrm{id}} + E_{\mathrm{iQ}} + E_{\mathrm{M}} \quad (2)$$

Here E_{nuc} corresponds to the combined nuclear relaxation of the charged molecule and the lattice; E_{dip} contains all static dipole moment interactions; E_{qQ} represents the interaction energy between the excess charge and the permanent quadrupole moments of the neighboring molecules (which is of particular importance for the molecules in this study); E_{id} denotes the energetic contributions from the induced-dipole moment interactions that modify the ionization potentials/electron affinities (to a first approximation, HOMO/LUMO energies); E_{iQ} is the extent of charge delocalization onto neighboring molecules; and E_{M} represents all contributions from higher-order multipole interactions.[12,14,15] We underline that the experimental and theoretical evaluation of intermolecular charge delocalization in oligoacene model systems is challenging and constitutes an active area of research, especially as it pertains to the proper physical description of charge-carrier transport in organic solids.[16−19] For instance, cluster-based studies of naphthalene suggest that both positive and negative charges delocalize over at least a few molecules,[14] which brings into question charge-hopping models that fully constrain the charges on single molecules; it is also worth noting that the amount of exact (nonlocal) exchange employed in commonly

Received: March 26, 2013
Revised: June 13, 2013
Published: June 14, 2013

Table 1. Representative Results[10,21,22,25] from Earlier Evaluations of Electronic Polarization Due to Positive (P_+) and Negative (P_-) Charges in Oligoacene Crystals[a]

		experiment[10]	INDO[22]	microelectrostatic[21]	QM/MM[25]
naphthalene	P_+/P_-	−1.72/−1.10			−1.93/−2.04
anthracene	P_+/P_-	−1.65/−1.09	−1.10/−1.10	−1.50/−	
pentacene	P_+/P_-	−1.63/−1.17	−1.03/−0.98	−1.45/−	−1.24/−1.49

[a]All energies are in eV.

used hybrid density functionals does greatly influence the theoretical description of charge delocalization.[20]

A number of theoretical approaches have been developed to describe electronic polarization in organic materials. These techniques range from classical microelectrostatic models[21] through semiempirical wave function methods[22,23] (e.g., intermediate neglect of differential overlap, INDO) to hybrid quantum-mechanics−molecular-mechanics (QM/MM) techniques.[24,25] The results from these approaches, however, generally suffer from limitations in describing the magnitude of the polarization, the asymmetry of the polarization as a function of the sign of the excess charge (that is, the difference between P_+ and P_-) and/or the magnitude of this asymmetry with respect to available experimental data, for instance for the oligoacene series; see Table 1.[10]

Here, our goal is to build on previous work[25,26] and employ an approach that makes use of a polarizable force field in order to describe the bulk polarization under vertical ionization conditions. From these calculations we extract exclusively the electronic polarization, i.e., the polarization energy neglecting nuclear motion. To demonstrate the general applicability of this model, we study the oligoacene crystal series (naphthalene through pentacene) and two perfluorinated acenes; the latter are of technological interest as perfluoropentacene behaves as an efficient n-channel transport material with electron transport mobilities up to 0.22 $cm^2\ V^{-1}\ s^{-1}$.[27] As the molecules under study do not present permanent dipole moments, multipole−quadrupole interactions become the primary electrostatic interactions in the neutral organic crystals. Hence, the atomic multipole optimized energetics for biomolecular applications (AMOEBA) force field[28−30] of Ponder and co-workers was chosen as the polarizable force field for the study as it includes multipole-quadrupole interactions through quantum-mechanically derived parameters and polarization is accounted for through the creation and interaction of induced dipoles with other static multipoles.

2. METHODOLOGY

The AMOEBA force field of Ponder and co-workers[28] is composed of eight energy components. The stretching, bending, out-of-plane bending, torsion, and stretch−bend terms are adopted from Allinger's MM3 force field,[31] while the van der Waals term is a dampened 14−7 Lennard-Jones potential.[32] The final two terms are electrostatic in nature and represent the permanent multipole and induced-dipole interactions. The permanent multipole interaction term (U_{elect}^{Perm}), eq 3, defines the influence of the multipole moments (M_i) of atom i on the multipole moments (M_j) of atom j through the operator T_{ij} given by eq 4:

$$U_{elec}^{Perm}(r_{ij}) = M_i^T T_{ij} M_j \tag{3}$$

$$T_{ij} = \begin{bmatrix} 1 & \frac{\partial}{\partial x_j} & \frac{\partial}{\partial y_j} & \frac{\partial}{\partial z_j} & \cdots \\ \frac{\partial}{\partial x_i} & \frac{\partial^2}{\partial x_i \partial x_j} & \frac{\partial^2}{\partial x_i \partial y_j} & \frac{\partial^2}{\partial x_i \partial z_j} & \cdots \\ \frac{\partial}{\partial y_i} & \frac{\partial^2}{\partial y_i \partial x_j} & \frac{\partial^2}{\partial y_i \partial y_j} & \frac{\partial^2}{\partial y_i \partial z_j} & \cdots \\ \frac{\partial}{\partial z_i} & \frac{\partial^2}{\partial z_i \partial x_j} & \frac{\partial^2}{\partial z_i \partial y_j} & \frac{\partial^2}{\partial z_i \partial z_j} & \cdots \\ \vdots & \vdots & \vdots & \vdots & \ddots \end{bmatrix} \left(\frac{1}{r_{ij}}\right) \tag{4}$$

where all interactions starting from charge−charge (1) to dipole−dipole ($\partial^2/\partial x_i \partial x_j$) interactions through quadrupole−quadrupole interactions as well as cross terms are taken into account.

Induced-dipole interactions in AMOEBA are calculated via eq 5 and are comprised of both direct and mutual induction

$$\mu_{i,\alpha}^{ind}(n+1) = (1-\omega)\mu_{i,\alpha}^{ind}(n) + \omega[\mu_{i,\alpha}^{ind}(0) + \alpha_i \Sigma_{\{j'\}} T_{\alpha\beta}^{ij'} \mu_{j',\beta}^{ind}(n)] \tag{5}$$

Direct induction, $\mu_{i,\alpha}^{ind}(0)$, is calculated as the induced-dipole component on atom i due to all static charge, dipole, and quadrupole moments that do not belong to the same polarization group; here, the polarization groups are defined as whole molecules. This direct induction is a function of the static electric field and as such does not vary. Mutual induction, however, does vary in response to changes of induced-dipole interactions. Mutual induction, $\alpha_i \sum_{\{j'\}} T_{\alpha\beta}^{ij'} \mu_{j',\beta}^{ind}(n)$, is calculated as the induced-dipole moment of atom i due to all other atomic induced-dipole moments of the other atoms, j', and is required to be summed over all atoms within the simulation in accordance with the Thole model.[33] The induction component is solved self-consistently in a successive-over-relaxation scheme where the factor ω controls the rate of convergence and α is the isotropic atomic polarizability.[34] To prevent the induced-dipole moment energy from going to infinity at short-range, a smearing function, ρ, is used to modify the dipole term of one site in the pair interaction

$$\rho = (3a/4\pi)\exp(-au^3) \tag{6}$$

This function effectively smears one charge distribution in each multipole interaction, as previously shown by Thole,[33,35] where u is the effective distance (a function of atomic polarizability) and a determines the damping strength.

Our studies of polarization in the oligoacenes were performed on the following crystal structures obtained from the Cambridge Structural Database (CSD identification codes are noted within the parentheses) with no further modification: naphthalene (NAPHTA06),[36] anthracene (ANTCEN09),[37]

tetracene (TETCEN01),[38] pentacene (PENCEN04),[39] perfluoronaphthalene (OFNAPH01),[40] and perfluoropentacene (BEZLUO)[41−43] The molecular geometries extracted from the experimental crystal structures and used in the single-molecule and cluster calculations are provided in the Supporting Information (SI).

To parametrize AMOEBA for the systems under consideration, a molecule was isolated/extracted from the respective crystals and single-particle density matrices for the neutral, radical-cation, and radical-anion states were determined through single-point energy calculations using second-order Møller−Plesset perturbation theory (MP2) and a 6-31+G(d,p) basis[44,45] as implemented in the *Gaussian 09* (revision A.02)[46] software suite.[47] As a check for accuracy, single-point coupled-cluster computations with single and double excitations (CCSD) were also carried out and show quantitatively modest and qualitatively no difference versus MP2 (see the SI for more detail) in terms of the charge distributions. Two important points to keep in mind is that the molecular geometries are "frozen" to those extracted from the crystals during the evaluations of the different redox states and that the subsequent electronic polarization energies determined through the methodology described here refer solely to those corresponding to vertical ionization processes (i.e., no molecular or lattice relaxation occurs, contributions that have been estimated to be a few tenths of an eV[12,25]), a constraint that allows us to focus solely on electronic polarization.

Using the MP2 density matrices, distributed multipole analyses were performed using the GDMA 2.2 software package[48] to obtain individual atom-centered charges (q_i), dipoles (μ_i), and quadrupoles (Q_i) in spherical tensor form for input into the AMOEBA force field. We note that the AMOEBA force field employs a Cartesian-based set of multipole tensors defined in a local coordinate frame and therefore transferable from molecule to molecule. This local coordinate frame is defined for each atom such that the origin is located at the atom of interest (i) with a directly bonded atom (j) defining the z axis. Then, an atom (k) adjacent to i is defined such that i−j−k forms an acute angle with the x axis lying in the i−j−k plane and the y axis perpendicular to the x and z axes. The tensors generated after rotation into the local coordinate frame were then inserted as new parameters in the AMOEBA force field as implemented in the Tinker 6.0[49] software suite. Atom types were defined using parameters from analogous atom classes when possible; otherwise, for atom classes not available in AMOEBA, parameters were adapted from the MM3 force field. The parameter sets optimized in this way are made available in the SI.

We then performed single-point energy calculations within Tinker using these new parameters, both for the isolated molecules and for clusters of varying sizes. Spherical clusters[50] were constructed where molecules with their center-of-mass inside a given radius were selected from a larger supercell and the charged molecule was set at the center of the cluster (Figure 1).

For calculations of the charged states, the atom types of the central molecule were replaced with those of the radical-anion or radical-cation species, whose parameters were defined in a way analogous to the neutral species. The polarization energies $P_{\pm}$ were then determined using the gas-phase and solid-state ionization potentials (IP)/electron affinities (EA) according to the Lyons definition (eq 1).

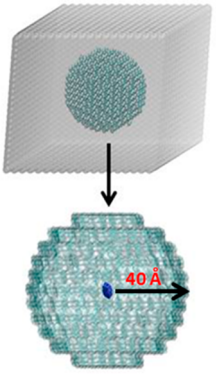

Figure 1. Naphthalene cluster (40 Å) cut from a larger supercell where the center-of-mass of the cluster is located at the center-of-mass of the molecule closest to the center of the supercell. The location of the charged naphthalene located at the center of the spherical cluster is shown in blue.

3. RESULTS AND DISCUSSION

The acenes, as noted above, present no permanent dipole moment; as a result, the quadrupole moment is the dominant component influencing intermolecular electrostatic interactions. For the acenes studied here, the herringbone packing motif found in the crystal leads to favorable positive-moment−negative-moment interactions among the quadrupole moments on neighboring molecules,[51] as schematically depicted in Figure 2 using the MP2/6-31+G(d,p)-derived values of isolated molecules. Importantly, as the redox state of the molecule changes, there is a large change in the electrostatic potential

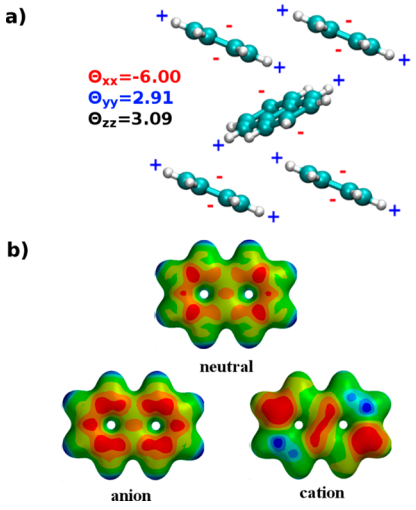

Figure 2. (a) Representation of the naphthalene crystal herringbone packing motif and quadrupole−quadrupole interactions for neutral molecules based on the quadrupole moments (Debye Å) calculated at the MP2/6-31+G(d) level for isolated, neutral naphthalene molecules. The quadrupole moments are given with respect to the normal (x), long (z), and short (y) axes. (b) Plots of the electrostatic potentials (ESPs, iso-surface value = 0.03 e/Å^3) for the neutral (top), radical-anion (bottom-left), and radical-cation (bottom-right) states of naphthalene in the neutral ground-state geometry at the MP2/6-31+G(d) level of theory. Red areas represent areas of electron accumulation, and blue areas show electron deficiency. Note that the naphthalene molecule extracted from the crystal has a modest geometric asymmetry that causes an asymmetry in the radical-cation ESP.

dx.doi.org/10.1021/jp402991z | J. Phys. Chem. C 2013, 117, 13853−13860

Table 2. Principal Quadrupole Moments (Debye Å) of the Neutral Oligoacenes As Determined at the MP2/6-31+G(d,p) Level of Theory and Using the Parameterized AMOEBA Force Field with Respect to the Normal (x), Long (z), and Short (y) Axes

	MP2			AMOEBA		
	θ_{xx}	θ_{yy}	θ_{zz}	θ_{xx}	θ_{yy}	θ_{zz}
naphthalene	−5.99	2.91	3.09	−2.96	1.36	1.59
	−14.36[a]	7.24[a]	7.11[a]			
	−13.31[b]	6.14[b]	7.17[b]			
anthracene	−8.29	3.80	4.50	−6.75	2.48	4.27
tetracene	−10.59	4.49	6.10	−7.41	2.45	4.96
pentacene	−12.93	5.59	7.34	−12.08	4.29	7.79
perfluoronaphthalene	6.71	−3.70	−3.01	22.30	−12.30	−9.96
perfluoropentacene	17.07	−8.61	−8.46	54.69	−29.04	−25.65

[a]Determined at the MP2/6-311++G(2d,2p)[25,53] level of theory and reported in ref 25. [b]Derived from theoretical calculations scaled to the experimental results of benzene in ref 52.

(ESP) profile of the molecule that in turn alters the interactions within the polarizable environment. We note that the naphthalene molecule extracted from the crystal (CSD identification NAPHTA06) has a modest twist along the backbone plane that induces a slight asymmetry in the ESP of the radical cation. For the radical anion, the ESPs show clear evidence of increased negative charge above/below the plane of the molecular backbone (i.e., π cloud of the aromatic structure); in the radical cation, there occurs a shift of the relative negative charge distribution to the ends (long axis) of the molecule. These shifts in electron density in turn affect the magnitude and sign of the multipole parameters (see the SI).

As was stated earlier, quadrupole moments are paramount to the description of oligoacene polarization in the solid state; the AMOEBA force field, therefore, must have the capacity to reproduce the (isolated) molecular quadrupole moments. Indeed, as shown in Table 2, the quadrupoles derived from the AMOEBA parameters optimized in this work present the same sign and relative magnitude as those from MP2, showing qualitative agreement. The AMOEBA-based data for naphthalene also compare favorably, if slightly smaller, to experimental data reported by Munn[52] and those previously reported at the MP2/6-311++G(2d,2p) level of theory.[25] For the perfluorinated species, we note that the AMOEBA-based quadrupole moments are significantly larger than those determined through the MP2 calculations; the cause of this disparity is not immediately evident, but the relative differences between the naphthalene/perfluoronaphthalene and pentacene/perfluoropentacene pairs are similar, and we therefore expect similar trends in the comparison. We recall that the charge-quadrupole interaction scales as $1/r^5$, so the differences between the AMOEBA quadrupole moments and those derived at the MP2 will have minor impact on the polarization energies.

We now turn to how the AMOEBA-based approach functions with regard to describing electrostatic interactions in the solid state. Using the basic (five-molecule) herringbone packing unit for naphthalene as a guide and taking the central molecule to carry an excess electron (Figure 3), the method produces differences in the induced-dipole moments on the exterior naphthalene molecules as expected due to the differences in position and orientation with respect to the central radical-anion naphthalene. The molecules that interact with the face of the central anion have a larger induced dipole (0.094 D) versus those neighbors that interact with the edge (0.084 D), i.e., a difference of 11%. When the central molecule is charged, the charge-quadrupole term becomes the dominant electrostatic interaction responsible for the polarization

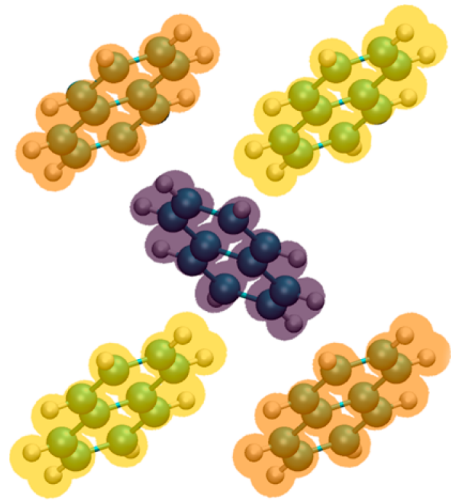

Figure 3. Magnitudes of the dipoles induced on the nearest molecules to a negatively charged naphthalene (central molecule). The molecules in yellow have induced dipoles of 0.094 D, and those in orange, of 0.084 D.

asymmetry.[54] Considering the relative molecular quadrupole orientations shown in Figure 2, the larger induced-dipole moments occur for the two molecules where the positive poles of the quadrupole points directly toward the central negative charge, and lead to the, albeit relatively small, asymmetry in the induced-dipole moments.

As the model is able to account for variations in electrostatic interactions in small model clusters, we now expand the investigation to probe the bulk electronic polarization in the acene crystals. As discussed in the Methodology section, a supercell was constructed from which spherical clusters were extracted by fixing the radius of the sphere at the center-of-mass of the molecule closest to the origin of the original unit cell within the supercell. The clusters we considered vary in size from a radius of 10 Å (~10 molecules) through radii of 30 to 40 Å (100s-1000s of molecules). This upper limit to the cluster size was determined reasonable as there is minimal change to the polarization energy as the cluster size increases beyond 40 Å; for instance, P_+ and P_- for naphthalene show differences of less than 0.02 eV between the 30 and 40 Å radii clusters, see Figure 4. As charge-quadrupole and induced dipole effects are short-range (both scale as $1/r^5$), the variations in polarization energy are larger for smaller clusters and then saturate for larger clusters. We note that for the larger clusters the change in the

dx.doi.org/10.1021/jp402991z | J. Phys. Chem. C 2013, 117, 13853−13860

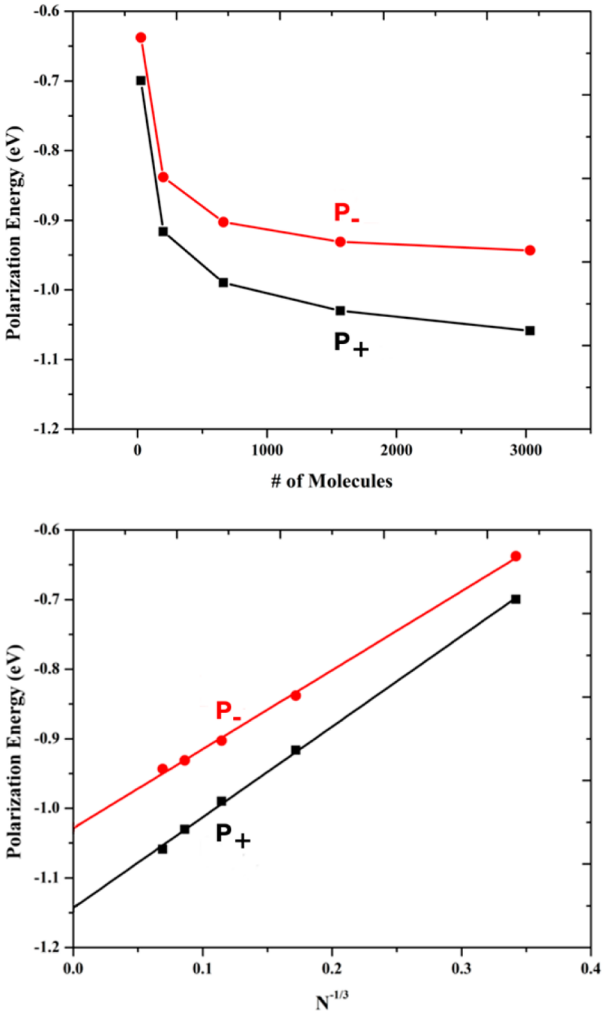

Figure 4. (Top) Polarization energy in naphthalene versus the number of molecules in the clusters. The points represent clusters of 10, 20, 30, 40, and 50 Å radii. There is about a 0.01 eV difference between the largest two clusters considered. (Bottom) Polarization energy plotted vs $N^{-1/3}$, where N is the number of molecules in the cluster.

polarization energy does remain mainly a function of induced-dipole interactions as these interactions act through a cascade effect that feeds through the system.

To determine the bulk polarization energies, the cluster polarization energies were extrapolated to infinity vs the inverse of the cube of the number of molecules in the cluster due to the spherical nature of the extracted systems ($N^{-1/3}$, Figures 4 and S2–S6). The polarization energies for the oligoacene series are presented in Table 3 alongside available experimental data.[10] Expanding the acene structure from naphthalene to anthracene through tetracene and pentacene, the characteristic trends observed experimentally emerge with the present model:

(i) The magnitude of P_+ decreases by 0.1 eV as the oligoacenes become larger from 1.14 eV in naphthalene to 1.02 eV in pentacene;

(ii) P_+ is more stabilizing than P_- due to the nature of the charge-quadrupole interactions, in agreement with the results of Bounds and Munn;[55,56]

(iii) The correct polarization asymmetry is obtained in view of the experimental data reported by Sato et al.[10]

Table 3. Comparison of Current Model and Experimental Data for Clusters of Naphthalene, Anthracene, Tetracene, Pentacene, and the Perfluorinated Species

	P_+ (eV)		P_- (eV)	
	this work	exp.[10]	this work	exp.[10]
naphthalene	−1.14	−1.72	−1.03	−1.10
anthracene	−1.11	−1.62	−0.85	−1.09
tetracene	−1.04	−1.63[a]	−0.92	−0.92[b]
pentacene	−1.02	−1.63	−0.79	−1.17
perfluoronaphthalene	−0.76		−1.18	
perfluoropentacene	−0.50		−1.27	

[a]References 57 and 58. [b]Reference 16.

The polarization energies for our calculations are of the same order of magnitude as those determined experimentally, increasing from 0.1 to 0.2 eV as the oligoacene length increases versus the 0.1−0.7 eV differences determined in earlier theoretical works.[21,22,25] We note, however, that the magnitude of the asymmetry is smaller in our calculations vs experiment, a function of the fact that our focus is solely on the electronic polarization and that we currently neglect potential stabilization from geometric and lattice relaxation, charge delocalization, and stabilizing charge penetration effects.[21,25] The inclusion of all or some of these effects may greatly increase the agreement between the model results and experimental evaluations.

To compare the current model with the earlier QM/MM method of ref 25, it is important to note the contrasting methods by which the charge and higher-order interactions are accounted. The QM/MM model used the self-consistent charge-equilibration scheme (QEq) scheme of Rappé and Goddard,[59] employing point charges located at atom centers and allowing them to fluctuate in response to a charged molecule. The point charges fluctuate based on a feedback loop with electronic-structure calculations where (i) the charged molecule is treated quantum mechanically, (ii) all other atoms are treated as charged points, and (iii) the values of these charged points equilibrate in a self-consistent fashion in response to the charge distribution on the quantum-mechanically treated molecule. Though this method allows for the net atomic charges representing the bulk material to fluctuate and in essence model polarization, it does not include terms for the quadrupole and induced-dipole interactions that Bounds and Munn[55,60] have shown to be necessary to accurately model the bulk polarization (especially in the oligoacenes).[61] The current model, however, does allow for interactions among charges, dipoles, and quadrupoles through a static picture that provides for the appropriate asymmetry of polarization in response to positive and negative charges. The lack of charge equilibration in our current model, though, can account somewhat for the smaller overall $P_\pm$ compared to the QM/MM model (Table 1).

We note that our current model and the previously implemented models all display a trend for P_ that is in relative disagreement with experimental results, namely a decrease of P_- with increasing oligoacene length. We observe a decrease of 0.24 eV in P_- compared to a very small increase of 0.07 eV measured via electron capture techniques; note that these values are smaller than the 0.5 eV experimental resolution, and that this trend may not be experimentally discernible.[62−64] The reason for the decreasing polarization energy has not been detailed in earlier work; as with the polarization energy due to a positive charge carrier, it is likely

dx.doi.org/10.1021/jp402991z | J. Phys. Chem. C 2013, 117, 13853−13860

an effect of the increased charge delocalization in the longer oligoacenes.

There is also intriguing evidence of an odd−even effect regarding the polarization asymmetry of the oligoacenes. Anthracene and pentacene (odd-numbered ring systems) show an asymmetry of 0.26 and 0.23 eV, respectively, while naphthalene and tetracene (even-numbered ring sytems) both have a polarization asymmetry that is 0.11 eV. The reason behind this odd−even effect is not clear at this time, but it is of interest that the systems with an even number of rings display one-half the polarization asymmetry as the odd-numbered ring structures.

We now turn our attention to the perfluorinated oligoacenes as a further test of the model. The strong electron-withdrawing nature of the fluorine atoms reverses the bond polarity for the C−F bond vs the C−H bond, leading to a reversal of sign of the principal quadrupole moments. These trends are evident when comparing the ESP maps of pentacene and perfluoropentacene (Figure 5).

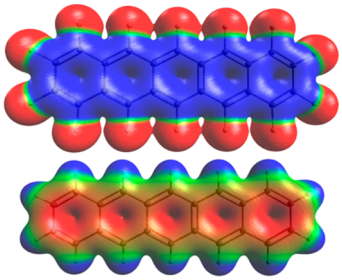

Figure 5. ESP map (iso-surface value = 0.03 $e/Å^3$) of pentacene (top) and perfluoropentacene (bottom) as determined at the MP2/6-31+G(d) level of theory. Red areas represent areas of electron accumulation and blue areas show electron deficiency.

For both perfluoronaphthalene and perfluoropentacene, P_- is more stabilizing than P_+ by more than 0.4 eV (Table 3); this is a direct function of the changes in sign of the principal quadrupole moments due to the substitution of the electron-withdrawing fluorine atoms (Table 2) that result in a change of sign in the charge-quadrupole interactions. We note there is also an apparent change in trend of the polarization energy as a function of the oligoacene length: perfluoronaphthalene has a larger P_+ versus perfluoropentacene, as is the case for the unsubstituted acenes, whereas P_- is larger for perfluoropentacene, in contrast with the trends of the unsubstituted acenes. As the number of perfluorinated systems experimentally available is limited, it is difficult to establish this trend, especially as consequences due to differences in polarization as a function of odd−even effects could be playing a role. It is our hope that these model calculations will spur interest in these systems leading to supportive experimental studies.

4. CONCLUSION

We have employed a methodology that makes use of a polarizable force field to evaluate the bulk electronic polarization energy due to the presence of a localized charge carrier in organic crystals. This method has been applied to unsubstituted and perfluorinated oligoacenes in order to demonstrate general applicability. As our focus was strictly on electronic polarization, effects due to geometric and lattice relaxation, charge delocalization, and charge penetration were not taken into account. These effects, in conjunction with that of the induced dipoles stressed here, are needed to obtain a more robust understanding of polarization, an area of active research in our group.

The electronic polarization energy results are in good qualitative agreement with experimental polarization energies both in terms of the magnitude and progression of the polarization energies when going from naphthalene to pentacene. The asymmetry of the P_+ and P_- polarization in oligoacenes is also qualitatively well described with respect to experimental data. On a more quantitative level, while the polarization asymmetries generated here are approximately a factor of 2−5 smaller than those observed experimentally, they are about three times larger than those given in earlier works based on INDO.[22] As out method correctly predicts the experimental trends, we expect the model used here to be generally applicable for the description of bulk polarization in organic molecular solids as well as polarization effects at materials interfaces, and that continued development of the model will lead to further agreement with experimental results.

■ ASSOCIATED CONTENT

Supporting Information

Coordinate files of the molecules used in these calculations, CCSD/MP2 charge comparisons, additional molecular-scale polarization data, and polarization energy extrapolations and a separate file with pertinent parameters developed here for the AMOEBA force field. This material is available free of charge via the Internet at http://pubs.acs.org.

■ AUTHOR INFORMATION

Corresponding Author

*E-mail: chad.risko@chemistry.gatech.edu; jean-luc.bredas@chemistry.gatech.edu.

Notes

The authors declare no competing financial interest.

‡Also affiliated with Department of Chemistry, King Abdulaziz University, Jeddah 21589, Saudi Arabia.

■ ACKNOWLEDGMENTS

This work was supported by the National Science Foundation through the MRSEC Program under Award DMR-0819885 with computing resources provided by the CRIF Program under Award CHE-0946869. We thank Professor C. Daniel Frisbie and Drs. David Beljonne, Jérôme Cornil, Veaceslav Coropceanu, Travis W. Kemper, and Michael S. Marshall for stimulating discussions.

■ REFERENCES

(1) Tang, C. W. Two-Layer Organic Photovoltaic Cell. *Appl. Phys. Lett.* **1986**, *48*, 183−185.

(2) Tang, C. W.; VanSlyke, S. A. Organic Electroluminescent Diodes. *Appl. Phys. Lett.* **1987**, *51*, 913−915.

(3) Garnier, F.; Horowitz, G.; Peng, X.; Fichou, D. An All-Organic "Soft" Thin Film Transistor with Very High Carrier Mobility. *Adv. Mater.* **1990**, *2*, 592−594.

(4) Burroughes, J. H.; Bradley, D. D. C.; Brown, A. R.; Marks, R. N.; Mackay, K.; Friend, R. H.; Burns, P. L.; Holmes, A. B. Light-Emitting Diodes Based on Conjugated Polymers. *Nature* **1990**, *347*, 539−541.

(5) O'Regan, B.; Gratzel, M. A Low-Cost, High-Efficiency Solar Cell Based on Dye-Sensitized Colloidal TiO_2 Films. *Nature* **1991**, *353*, 737−740.

(6) Kippelen, B.; Bredas, J. L. Organic Photovoltaics. *Energy Environ. Sci.* **2009**, *2*, 251−261.

(7) Lyons, L. E. Photo- and Semi-Conductance in Organic Crystals. Part V. Ionized States in Molecular Crystals. *J. Chem. Soc.* **1957**, 5001−5007.
(8) Silinsh, E. A. *Organic Molecular Crystals: Their Electronic States*; Springer: New York, 1978.
(9) Sato, N.; Seki, K.; Inokuchi, H. Polarization Energies of Organic-Solids Determined by Ultraviolet Photoelectron-Spectroscopy. *J. Chem. Soc., Faraday Trans. 2* **1981**, *77*, 1621−1633.
(10) Sato, N.; Inokuchi, H.; Silinsh, E. A. Reevaluation of Electronic Polarization Energies in Organic Molecular Crystals. *Chem. Phys.* **1987**, *115*, 269−277.
(11) Griffith, O. L.; Anthony, J. E.; Jones, A. G.; Shu, Y.; Lichtenberger, D. L. Substituent Effects on the Electronic Characteristics of Pentacene Derivatives for Organic Electronic Devices: Dioxolane-Substituted Pentacene Derivatives with Triisopropylsilylethynyl Functional Groups. *J. Am. Chem. Soc.* **2012**, *134*, 14185−14194.
(12) Silinsh, E. A.; Capek, V. *Organic Molecular Crystals: Interaction, Localization, and Transport Phenomena*; AIP: New York, 1994.
(13) See ref 12, p 125.
(14) Saigusa, H.; Lim, E. C. Photodissociation Spectra of Naphthalene Cluster Ions $(C_{10}H_8)_N^+$, N = 2−7: Evidence for Dimer Core Structure and Comparison with Neutral Clusters. *J. Phys. Chem.* **1994**, *98*, 13470−13475.
(15) The systems of interest here have no static dipole moments, and the higher-order multipoles are expected to be a small correction and thus have been omitted.
(16) Ando, N.; Mitsui, M.; Nakajima, A. Photoelectron Spectroscopy of Cluster Anion of Naphthalene and Related Aromatic Hydrocarbons. *J. Chem. Phys.* **2008**, *128*, 154318.
(17) Martinelli, N. G.; Ide, J.; Sanchez-Carrera, R. S.; Coropceanu, V.; Bredas, J. L.; Ducasse, L.; Castet, F.; Cornil, J.; Beljonne, D. Influence of Structural Dynamics on Polarization Energies in Anthracene Single Crystals. *J. Phys. Chem. C* **2010**, *114*, 20678−20685.
(18) Minder, N. A.; Ono, S.; Chen, Z.; Facchetti, A.; Morpurgo, A. F. Band-Like Electron Transport in Organic Transistors and Implication of the Molecular Structure for Performance Optimization. *Adv. Mater.* **2012**, *24*, 503−508.
(19) Liu, T.; Cheung, D. L.; Troisi, A. Structural Variability and Dynamics of the P3ht/Pcbm Interface and Its Effects on the Electronic Structure and the Charge-Transfer Rates in Solar Cells. *Phys. Chem. Chem. Phys.* **2011**, *13*, 21461−21470.
(20) Sai, N.; Barbara, P. F.; Leung, K. Hole Localization in Molecular Crystals from Hybrid Density Functional Thoery. *Phys. Rev. Lett.* **2011**, *106*, 226403.
(21) Verlaak, S.; Heremans, P. Molecular Microelectrostatic View on Electronic States near Pentacene Grain Boundaries. *Phys. Rev. B: Condens. Matter* **2007**, *75*, 115127.
(22) Soos, Z. G.; Tsiper, E. V.; Pascal, R. A., Jr. Charge Redistribution and Electronic Polarization in Organic Molecular Crystals. *Chem. Phys. Lett.* **2001**, *342*, 652−658.
(23) Tsiper, E. V.; Soos, Z. G. Electronic Polarization in Pentacene Crystals and Thin Films. *Phys. Rev. B: Condens. Matter* **2003**, *68*, 085301.
(24) Difley, S.; Wang, L.-P.; Yeganeh, S.; Yost, S. R.; Voorhis, T. V. Electronic Properties of Disordered Organic Semiconductors Via Qm/Mm Simulations. *Acc. Chem. Res.* **2010**, *43*, 995−1004.
(25) Norton, J. E.; Brédas, J.-L. Polarization Energies in Oligoacene Semiconductor Crystals. *J. Am. Chem. Soc.* **2008**, *130*, 12377−12384.
(26) The main approach employed in the previous work was built from a QM/MM scheme that used fluctuating charges to model polarization. Trends concerning the order of the polarization as a function of the sign of the charge carrier derived from this approach, however, were inconsistent with experimental results.
(27) Sakamoto, Y.; Suzuki, T.; Kobayashi, M.; Yuan, G.; Inoue, Y.; Tokito, S. Perfluoropentacene and Perfluorotetracene: Syntheses, Crystal Structures, and Fet Characteristics. *Mol. Cryst. Liq. Cryst.* **2006**, *444*, 225−232.
(28) Ren, P.; Ponder, J. W. Consistent Treatment of Inter- and Intramolecular Polarization in Molecular Mechanics Calculations. *J. Comput. Chem.* **2002**, *23*, 1497−1506.
(29) Ren, P.; Ponder, J. W. Polarizable Atomic Multipole Water Model for Molecular Mechanics Simulation. *J. Phys. Chem. B* **2003**, *107*, 5933−5947.
(30) Ponder, J. W.; Wu, C.; Ren, P.; Pande, V. S.; Chodera, J. D.; Schnieders, M. J.; Haque, I.; Mobley, D. L.; Lambrecht, D. S.; DiStasio, R. A.; Head-Gordon, M.; Clark, G. N. I.; Johnson, M. E.; Head-Gordon, T. Current Status of the Amoeba Polarizable Force Field. *J. Phys. Chem. B* **2010**, *114*, 2549−2564.
(31) Allinger, N. L.; Yuh, Y. H.; Lii, J. H. Molecular Mechanics - the MM3 Force-Field for Hyrdocarbons. 1. *J. Am. Chem. Soc.* **1989**, *111*, 8551−8566.
(32) Patel, S.; Brooks, C. L. Charmm Fluctuating Charge Force Field for Proteins: I Parameterization and Application to Bulk Organic Liquid Simulations. *J. Comput. Chem.* **2004**, *25*, 1−15.
(33) Thole, B. T. Molecular Polarizabilities Calculated with a Modified Dipole Interaction. *Chem. Phys.* **1981**, *59*, 341−350.
(34) Young, D. M. *Iterative Solution of Large Linear Systems*; Academic Press: New York, 1971.
(35) van Duijnen, P. T.; Swart, M. Molecular and Atomic Polarizabilities: Thole's Model Revisited. *J. Phys. Chem. A* **1998**, *102*, 2399−2407.
(36) Brock, C. P.; Dunitz, J. D. Temperature-Dependence of Thermal Motion in Crystalline Naphthalene. *Acta Crystallogr., Sect. B* **1982**, *B38*, 2218−2228.
(37) Brock, C. P.; Dunitz, J. D. Temperature-Dependence of Thermal Motion in Crystalline Anthracene. *Acta Crystallogr., Sect. B* **1990**, *B46*, 795−806.
(38) Holmes, D.; Kumaraswamy, S.; Matzger, A. J.; Vollhardt, K. P. C. On the Nature of Nonplanarity in the [N]Phenylenes. *Chem.−Eur. J.* **1999**, *5*, 3399−3412.
(39) Mattheus, C. C.; Dros, A. B.; Baas, J.; Meetsma, A.; Boer, J. L. d.; Palstra, T. T. M. Polymorphism in Pentacene. *Acta Crystallogr., Sect. C: Cryst. Struct. Commun.* **2001**, *57*, 939−941.
(40) Akhmed, N. A. Study of Crystalline-Structure of Octafluoronaphthalene. *Russ. J. Struct. Chem.* **1973**, *14*, 573−574.
(41) Sakamoto, Y.; Suzuki, T.; Kobayashi, M.; Gao, Y.; Fukai, Y.; Inoue, Y.; Sato, F.; Tokito, S. Perfluoropentacene: High-Performance P-N Junctions and Complementary Circuits with Pentacene. *J. Am. Chem. Soc.* **2004**, *126*, 8138−8140.
(42) Allen, F. H. The Cambridge Structural Database: A Quarter Million Crystal Structures and Rising. *Acta Crystallogr. Sect. B: Struct. Sci.* **2002**, *58*, 380−388.
(43) Fletcher, D. A.; McMeeking, R. F.; Parkin, D. The United Kingdom Chemical Database Service. *J. Chem. Inf. Comput. Sci.* **1996**, *36*, 746−749.
(44) Rick, S. W.; Stuart, S. J. Potentials and Algorithms for Incorporating Polarizability in Computer Simulations. *Rev. Comput. Chem.* **2002**, *18*, 89−146.
(45) Halgren, T. A.; Damm, W. Polarizable Force Fields. *Curr. Opin. Struct. Biol.* **2001**, *11*, 236−242.
(46) Frisch, M. J.; Trucks, G. W.; Schlegel, H. B.; Scuseria, G. E.; Robb, M. A.; Cheeseman, J. R.; Scalmani, G.; Barone, V.; Mennucci, B.; Petersson, G. A.; Nakatsuji, H.; Caricato, M.; Li, X.; Hratchian, H. P.; Izmaylov, A. F.; Bloino, J.; Zheng, G.; Sonnenberg, J. L.; Hada, M.; Ehara, M.; Toyota, K.; Fukuda, R.; Hasegawa, J.; Ishida, M.; Nakajima, T.; Honda, Y.; Kitao, O.; Nakai, H.; Vreven, T.; Montgomery, J. A.; Peralta, J. E.; Ogliaro, F.; Bearpark, M.; Heyd, J. J.; Brothers, E.; Kudin, K. N.; Staroverov, V. N.; Kobayashi, R.; Normand, J.; Raghavachari, K.; Rendell, A.; Burant, J. C.; Iyengar, S. S.; Tomasi, J.; Cossi, M.; Rega, N.; Millam, J. M.; Klene, M.; Knox, J. E.; Cross, J. B.; Bakken, V.; Adamo, C.; Jaramillo, J.; Gomperts, R.; Stratmann, R. E.; Yazyev, O.; Austin, A. J.; Cammi, R.; Pomelli, C.; Ochterski, J. W.; Martin, R. L.; Morokuma, K.; Zakrzewski, V. G.; Voth, G. A.; Salvador, P.; Dannenberg, J. J.; Dapprich, S.; Daniels, A. D.; Farkas, O.; Foresman, J. B.; Ortiz, J. V.; Cioslowski, J.; Fox, D. J. *Gaussian 09*, revision B.01; Gaussian Inc.: Wallingford, CT, 2009.

(47) We note that the 6-31+G(d,p) basis was chosen to provide the capability to scale the method described here to larger systems.
(48) Stone, A. J. Distributed Multipole Analysis: Stability for Large Basis Sets. *J. Chem. Theory Comput.* **2005**, *1*, 1128−1132.
(49) Ponder, J. W. *Tinker: Software Tools for Molecular Design, 6.0.* 2012.
(50) We note that care needs to be taken during construction of the clusters as even slight asymmetry can lead to spurious results.
(51) Williams, J. H. The Molecular Electric Quadrupole Moment and Solid-State Architecture. *Acc. Chem. Res.* **1993**, *26*, 593−598.
(52) Eisenstein, I.; Munn, R. W. Polarization Energy of a Localized Charge in a Molecular Crystal. V. Effect of Vacancies. *Chem. Phys.* **1983**, *77*, 47−61.
(53) Calculated multipole moments were derived from distributed multipole analysis of the calculated wave function by the GDMA program of A. Stone.
(54) In these charged systems the charge-quadrupole interaction will be the primary interaction that results in asymmetry of the polarization energy, and the splitting will of opposite signs for holes and electrons. This splitting, though, may not be equivalent depending on the charge distribution along the molecule.
(55) Bounds, P. J.; Munn, R. W. Polarization Energy of a Localized Charge in a Molecular Crystal. Ii. Charge-Quadrupole Energy. *Chem. Phys.* **1981**, *59*, 41−45.
(56) The charge interaction energy is proportional to the charge on the species multiplied by the quadrupole moment and divided by the distance between the quadrupole point and the charge point.
(57) Pope, M.; Burgos, J.; Giachino, J. Charge-Transfer Exciton State and Energy Levels in Tetracene Crystal. *J. Chem. Phys.* **1965**, *43*, 3367−3371.
(58) Berry, R. S.; Jortner, J.; Mackie, J. C.; Pysh, E. S.; Rice, S. A. Search for a Charge-Transfer State in Crystalline Anthracene. *J. Chem. Phys.* **1965**, *42*, 1535−1540.
(59) Rappé„ A. K.; Goddard, W. A. Charge Equilibration for Molecular-Dynamics Simulations. *J. Phys. Chem.* **1991**, *95*, 3358−3363.
(60) Bounds, P. J.; Munn, R. W. Polarization Energy of a Localized Charge in a Molecular Crystal. *Chem. Phys.* **1979**, *44*, 103−112.
(61) It should be noted that quadrupole and induced dipole interactions are indirectly accounted for in the Qeq model, but the quality of these interactions is questionable. For point charge models it is difficult, if not impossible, to reproduce the quadrupoles of molecular systems with even qualitative accuracy. Because of this defficiency the quadrupoles in the Qeq model are most likely qualitatively incorrect, and therefore, the mignitude of the quadrupoles, induced dipoles, and quadrupole-induced dipole interactions are likely incorrect leading to the reversal of the polarization energy observed.
(62) Lyons, L. E.; Morris, G. C.; Warren, L. J. Electron Affinities and the Electron-Capture Method for Aromatic Hydrocarbons. *J. Phys. Chem.* **1968**, *72*, 3677−3678.
(63) Wentworth, W. E.; Chen, E. Lovelock, J. E., The Pulse-Sampling Technique for the Study of Electron-Attachment Phenomena. *J. Phys. Chem.* **1966**, *70*, 445−458.
(64) Lyons, L.; Morris, G.; Warren, L. The Measurement of Electron Affinities by the Gaseous Electron Capture Technique. *Aust. J. Chem.* **1968**, *21*, 853−871.